Microwave Sintering Studies at 2.45 GHz

A.W. Fliflet
R.P. Fischer

Beam Physics Branch
Plasma Physics Division

D. Lewis, III
R.J. Rayne
B.D. Bender
G.-M. Chow

Mechanics of Materials Branch
Materials Science and Technology Division

P.E. Schoen

Center for Biomolecular Science and Engineering

R.W. Bruce
A.K. Kinkead

Sachs Freeman Associates, Inc.
Largo, MD 20774

L.K. Kurihara

Georgetown University
Washington, DC 20057

[DTIC QUALITY INSPECTED 3

July 20, 1997

19970820 145

REPORT DOCUMENTATION PAGE

Public reporting burden for this collection of information is estimated to average 1 hour per response, including the time for reviewing instructions, searching existing data sources, gathering and maintaining the data needed, and completing and reviewing the collection of information. Send comments regarding this burden estimate or any other aspect of this collection of information, including suggestions for reducing this burden, to Washington Headquarters Services, Directorate for Information Operations and Reports, 1215 Jefferson Davis Highway, Suite 1204, Arlington, VA 22202-4302, and to the Office of Management and Budget. Paperwork Reduction Project (0704-0188), Washington, DC 20503.

1. AGENCY USE ONLY (Leave Blank)	2. REPORT DATE July 20, 1997	3. REPORT TYPE AND DATES COVERED Interim	
4. TITLE AND SUBTITLE Microwave Sintering Studies at 2.45 GHz			**5. FUNDING NUMBERS**
6. AUTHOR(S) A.W. Fliflet, R.W. Bruce,* R.P. Fischer, A.K. Kinkead,* D. Lewis, III,** R.J. Rayne,** B.D. Bender,** G.M. Chow,** L.K. Kurihara,*** and P.E. Schoen†			

7. PERFORMING ORGANIZATION NAME(S) AND ADDRESS(ES) Naval Research Laboratory Washington, DC 20375-5320	8. PERFORMING ORGANIZATION REPORT NUMBER NRL/MR/6793--97-7959
9. SPONSORING/MONITORING AGENCY NAME(S) AND ADDRESS(ES) Office of Naval Research 800 North Quincy Street Arlington, VA 22217-5660	10. SPONSORING/MONITORING AGENCY REPORT NUMBER

11. SUPPLEMENTARY NOTES
*Sachs Freeman Associates, Inc., Largo, MD 20774
**NRL, Materials Science & Technology Division
***Georegtown University, Washington, DC 20057
†NRL, Center for Biomolecular Science and Engineering

12a. DISTRIBUTION/AVAILABILITY STATEMENT Approved for public release; distribution unlimited.	12b. DISTRIBUTION CODE

13. ABSTRACT (Maximum 200 words)

    Microwave sintering studies of oxide ceramics have been conducted at 2.45 GHz. A single-mode cavity microwave furnace, operating in the TE_{103} mode, was used to investigate sintering of pure and doped nanocrystalline alumina. The purpose of these experiments was to determine the effect of additives on the sintering process in the nanocrystalline regime. The optimization of insulating casket and susceptor systems was also investigated.

14. SUBJECT TERMS Microwave Sintering Nanocrystalline ceramics			15. NUMBER OF PAGES 34
			16. PRICE CODE

17. SECURITY CLASSIFICATION OF REPORT UNCLASSIFIED	18. SECURITY CLASSIFICATION OF THIS PAGE UNCLASSIFIED	19. SECURITY CLASSIFICATION OF ABSTRACT UNCLASSIFIED	20. LIMITATION OF ABSTRACT SAR

CONTENTS

Microwave Sintering Studies at 2.45 GHz

I. Introduction

Microwave processing of advanced ceramic materials is emerging as an important new technology with many advantages compared to conventional processing techniques. In conventional heating of ceramic materials, energy is applied at the surface of the workpiece by flowing gas or infrared radiation and is transferred into the bulk by conduction. This process is necessarily slow (the processing time is usually measured in hours) because of the need to avoid internal stresses in the material due to the nonuniform heating process, and the large thermal mass of the furnace itself. In the case of ceramic sintering—the process by which polycrystalline ceramic compacts are densified and strengthened—the desired shrinkage and elimination of inter-grain volume, or "pores," is often accompanied by significant grain growth, resulting in reduced material performance. Microwave heating is of interest because it deposits energy volumetrically, and can produce rapid heating rates, resulting in less grain growth and more efficient processing. On the other hand, since the microwave absorption rate is highly temperature dependent and ceramic materials usually have low heat conductivity, the heating process, if not carefully monitored and controlled, is prone to temporal and spatial instabilities which lead to thermal runaway and cause local melting or cracking. In addition, the microwave absorption coefficient of 2.45 GHz radiation (the frequency of conventional microwave ovens) for many ceramic materials at room temperature is so low that heating cannot be achieved without using hybrid (conduction + microwave) heating techniques.

Nanocrystalline ceramics are composed of ultrafine-grained particles (grain size, $d \sim 10\text{--}100$ nm) and are expected to have unique material properties if processing issues can be successfully resolved. This is because material strength increases with decreasing grain size, as does its plasticity at high temperatures—a property which determines the ability to affect the final shape of sintered materials. The ratio of surface area to volume is much higher in nanocrystalline materials than in conventional polycrystalline ceramics so that surface tension, the driving force in sintering, is very strong. On one hand, this means that the process can be rapid and can occur at lower temperatures, but on the other hand, nanopowders are prone to form agglomerates, or particle clusters, which degrade the sintered material by promoting grain growth during densification. The potential for controlled rapid heating using microwaves makes it particularly attractive for sintering these nanocrystalline ceramics.

The microwave sintering and densification of nanocrystalline alumina compacts is of current research interest [1-7]. One of the goals of the present work was to study the effect of the doping of very pure nanocrystalline alumina on the heating, sintering and densification of this material. The addition of dopants (i.e., sintering aids) has been a long standing practice of the ceramics industry for achieving higher densification at lower temperatures than would be achieved with the pure material. A previous NRL study using a 2.45 GHz single-mode microwave furnace focused on very pure materials [1]. The results were disappointing as these compacts required relatively high temperatures to achieve significant densification, and the final grain sizes were large, typically several microns. These problems were attributed to the agglomeration of the nanocrystalline grains apparent in the green compacts [1-2]. Agglomerates impede the sintering process by reducing the green compact density and by favoring grain growth over densification. Another study, by Freim, et. al., has emphasized the importance of the γ to α phase transition as a cause of the anomalous grain growth during sintering of nanocrystalline alumina [7]. Unfortunately, our present results, given in Section II, indicate that although the dopants can decrease the temperature needed for achieving a given density, the sintering process remains dominated by the presence of these agglomerates.

This memo also presents a optimization study of the casket used to insulate the workpiece from the surrounding cold-walled microwave furnace. In addition to providing insulation, the casket can provide hybrid heating at low workpiece temperatures. However, microwave energy deposition in the casket material can lead to casket hot spots and thermal runaway, resulting in destruction of the casket and uncontrolled workpiece temperatures. A discussion of the various susceptor/insulator schemes devised to ensure successful sintering of the nanocrystalline compacts is given in Section III. A summary and discussion of our results to date is presented in Section IV.

II.   Sintering Experiments

A.   *2.45 GHz Single-mode Microwave Furnace*

The NRL 2.45 GHz microwave furnace system consists of a microwave source, waveguide transmission and control devices, a single-mode resonant cavity, and power and temperature sensors. The purpose of the microwave cavity and associated hardware is to maximize the electric field at the workpiece and optimize the microwave coupling efficiency. As the workpiece heats, its electrical properties change, and it is necessary to adjust the cavity dimensions to maintain resonance and effective power coupling. The system is powered by a Cober S6F 2.45 GHz industrial magnetron which can produce up to 6 kW of continuous wave (CW) power.

The principal problems encountered in setting up the furnace were associated with control of the incident power, monitoring of the forward and reflected power, and the wide variation of the load impedance during heating. Measurement of the forward and reflected power is necessary to monitor power flow into the cavity and to keep the cavity tuned to resonance. Because the load impedance varies greatly during the heating/sintering process, the ability to monitor how well the source is matched to the cavity is of great importance. The Cober microwave source could not be operated stablely at output powers below 600 W, requiring the addition of a variable power divider. During initial experiments, the power incident to the cavity applicator was moderated only by the movement of the variable short, and the initial temperature rise of the workpiece was very rapid and difficult to control. With the variable power divider, the cavity could be brought into resonance at low power and the power then raised slowly to more controllably reach the desired temperature. Additional control, and improved coupling efficiency, was obtained adding a variable diaphragm at the cavity input. A circulator was also added to the system downstream from the power divider since reflected power was found to interfere with the power divider operation. The microwave cavity is designed to support the TE_{103} rectangular waveguide mode and is constructed from WR-284 copper waveguide (a = 7.21 cm, b = 3.40 cm). There is an adjustable diaphragm (iris) at one end for power input, and a sliding short at the other.

B. *Sample Preparation*

Nanocrystalline powders were prepared using a modified sol-gel technique [8]. The precursor alkoxide was suspended in absolute ethanol while stirring. A solution of distilled de-ionized water (DDW) - ethanol (excess water) was made into an aerosol with nitrogen and sprayed into the alkoxide suspension. The reactants were stirred for an additional 30 minutes after the addition of the water solution and then filtered, washed with water and dried. The precursor powders were calcined in air at 700°C for 2 hours to remove the organic moieties. The dopants were either added during the sol-gel synthesis (in solution) or after calcination (as powder). The x-ray diffraction patterns for each of the calcined powders are given in Figure 1. These patterns indicate that the calcined powders were nanocrystalline (< 5 nm) γ-alumina with the additives appearing as microcrystalline peaks only for the nanocrystalline alumina with yttria.

These powders were then uniaxially pressed to 35 MPa and cold isostatically pressed (CIP'ed) to 414 MPa, producing 1.00 cm diameter, 0.63 cm high cylindrical compacts. Initial green densities are given in Table I. The samples were placed in a box oven at 200°C until the sintering operation to minimize the absorption of water vapor prior to sintering.
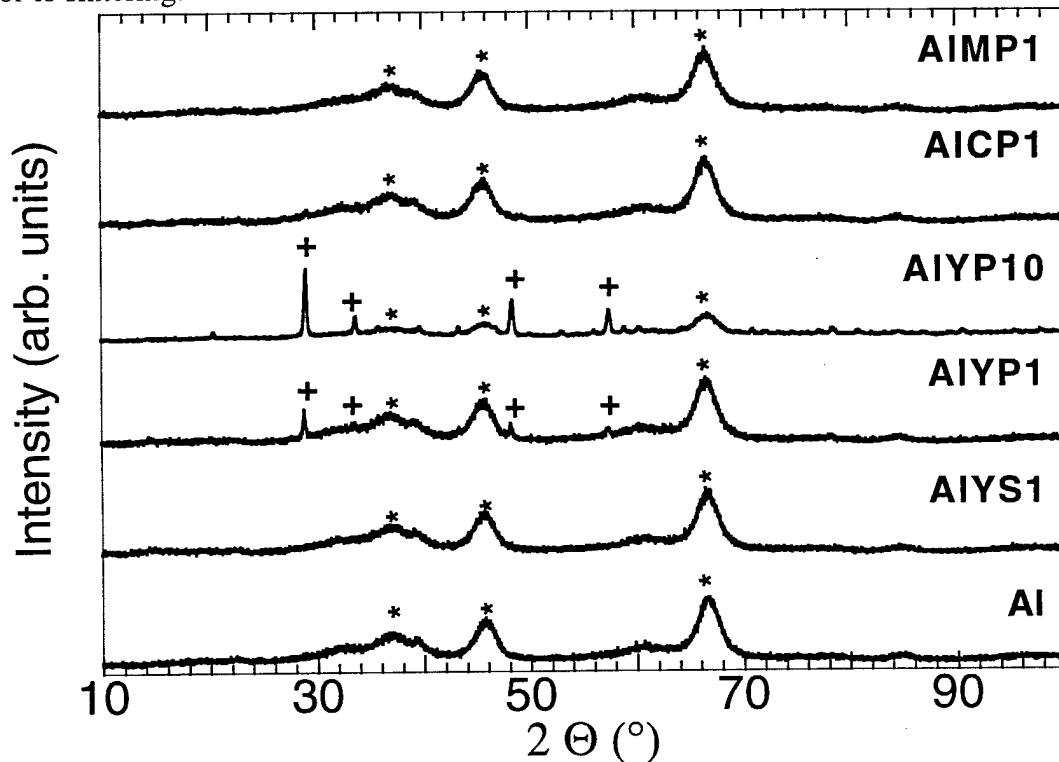

Figure 1. X-ray diffraction plots of the calcined powders. Legend: *: γ-alumina peaks; +: yttria (Y_2O_3) peaks

Table I: Designation of Powders

Sample Designation	Dopant	Initial Rel. Density	Initial Grain Size
Al	Pure	41.5%	3.8 nm
AlYS1	1 wt% Y_2O_3 added in solution	41.0%	4.0 nm
AlYP1	1 wt% Y_2O_3 added as powder	42.2%	3.9 nm
AlYP10	10 wt% Y_2O_3 added as powder	42.1%	3.8 nm
AlCP1	1 wt% CaO added as powder	43.3%	3.4 nm
AlMP1	1 wt% MgO added as powder	43.4%	3.2 nm

## C.   Sintering Procedure, Control and Measurement

Each sample was placed in a casket made from fiber insulation and/or a susceptor material as discussed in Section III[9]. The casket assembly was then placed near the center maxima of the TE_{103} microwave furnace. Runs with various heating profiles were then made to determine the final densities that could be obtained at various peak temperatures (typically 1100°C through 1800°C) and dwell times (typically 0 to 30 minutes). The microwave power was increased during the run to bring the sample up to temperature in approximately 15 minutes. The cooling time of the samples was approximately 15 minutes. All sintering runs were done in air at one atmosphere of pressure. Surface temperature was monitored through a hole in the casket using a two-color pyrometer (Mikron^{TM} M190R). Pyrometer temperature measurements were calibrated to a thermocouple using a tube furnace and nanocrystalline alumina compacts as the standard material. Figure 2 shows the range of results for the sintering of nano Al_2O_3 with 10 wt% Y_2O_3. A detailed discussion of the density of these samples as a function of temperature is given in the next section. Figure 2 shows that significant densification and size reduction is obtainable at 2.45 GHz. Area decreases from the unprocessed sample (Control) of 0.87 cm^2 to 0.47 cm^2 for the 1747°C sample (#6). Although the conventionally sintered sample (C1) was slightly more dense than was the microwave sample (#1) at 1100°C (52% TD vs. 47% TD), the microwave sample (#5) was significantly more dense at ~1500°C than the conventional sample (C2) (73% TD vs. 63%TD).

D. *Results and Discussion*

1. Densification during Sintering

The green and sintered densities were calculated from the weight and dimensions of the compacts. The relative density of the sintered compacts as a function of peak surface temperature is plotted in Figure 3(A) for pure alumina and alumina with 10 wt% yttria. The data of Freim et al. for sintering of commercially available gas condensation synthesized nanocrystalline γ-alumina is shown for comparison [7]. Sintered densities ranged from little change for the lowest processing temperatures (~1100°C) to over 90% relative density for temperatures >1700°C. Densification data for nanocrystalline alumina with other dopants is shown in Figure 4. The scatter in these data is attributed mainly to problems of non-uniform heating and thermal runaway in the somewhat lossy casket material. These effects could result in the interior temperature of the sample being substantially different from the monitored surface temperature. Severe cases of thermal runaway led to melting of the casket material and shifting of the sample. Improvements in casket design were implemented while these data were being obtained as discussed in Section III and Ref. 9.

As expected, the NRL pure nanocrystalline material shows the least amount of densification at a given temperature. Among the doped materials, the samples containing Y_2O_3 densified the most with the 10 wt% samples achieving the highest values [Figure 3(A)]. Comparison of our data with the data of Ref. 7 for pure nanocrystalline alumina shows significantly less densification for our compacts particularly at the lower temperatures. This is attributed to the lower starting densities (42% versus 55% relative density) of our compacts even though they were cold-pressed at higher pressure than the compacts prepared in Ref. 7 (414 vs. 350 MPa). This difference in initial density may be caused by an increased agglomeration or polydispersion of our powders. When these data and the Ref. 7 data are compared to conventional sintering data obtained by Coble [10], the results are very similar in the 1400 to 1600 °C temperature regime though the processing times were significantly less: 5 minutes for the nanocrystalline material versus 60 minutes for Coble's microcrystalline material.

6

CM
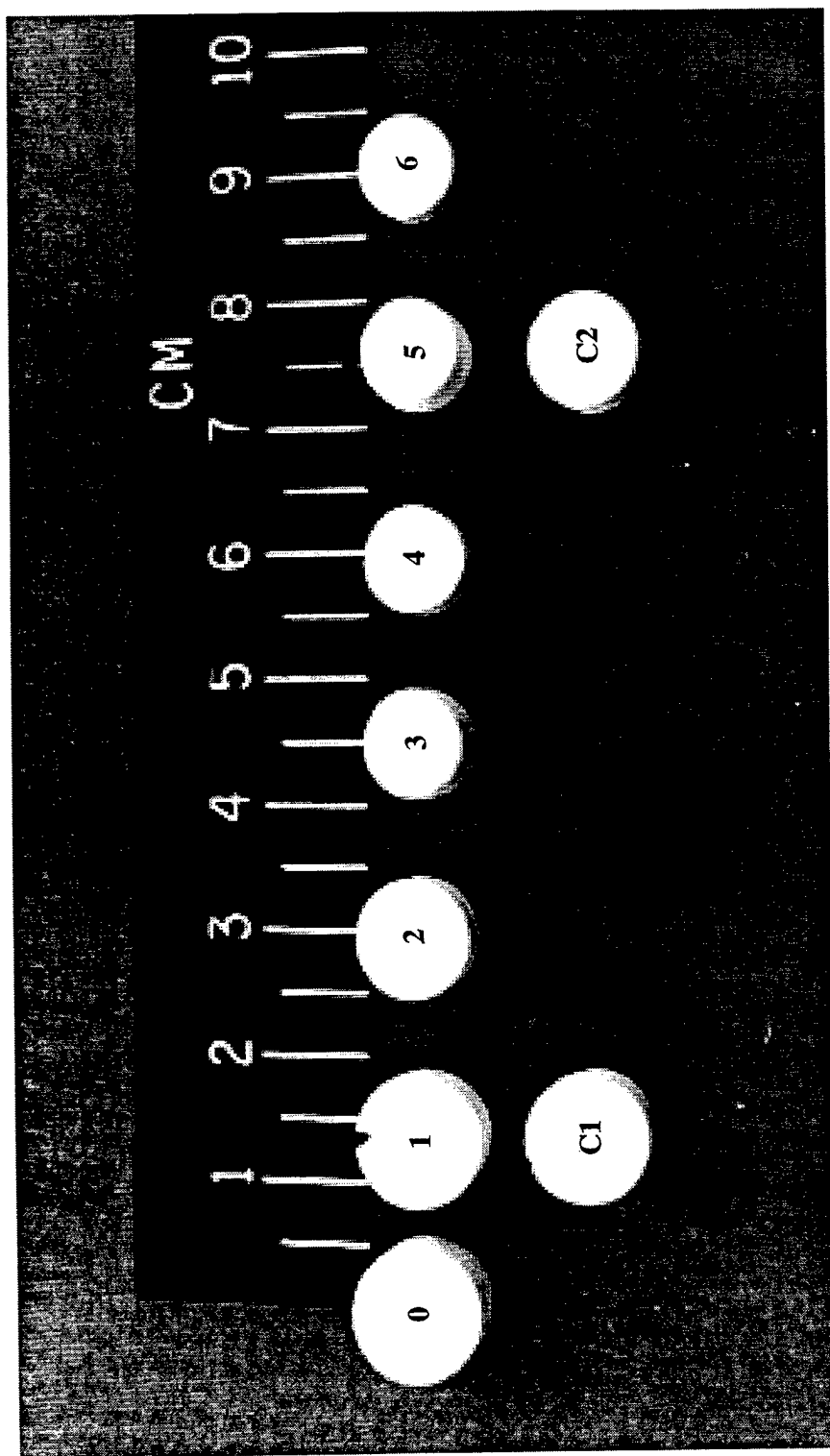
Sample				
0:	Control: nano Al_2O_3 (γ)		42 % TD	Unprocessed, initial density
1:	nano Al_2O_3 (γ) with 10 wt% Y_2O_3;	1100°C; 0 min dwell;	47 % TD	2.45 GHz Microwave
2:	nano Al_2O_3 (α) with 10 wt% Y_2O_3;	1200°C; 30 min dwell;	56 % TD	2.45 GHz Microwave
3:	nano Al_2O_3 (α) with 10 wt% Y_2O_3;	1400°C; 0 min dwell;	69 % TD	2.45 GHz Microwave
4:	nano Al_2O_3 (α) with 10 wt% Y_2O_3;	1450°C; 30 min dwell;	77 % TD	2.45 GHz Microwave
5:	nano Al_2O_3 (α) with 10 wt% Y_2O_3;	1520°C; 0 min dwell;	73 % TD	2.45 GHz Microwave
6:	nano Al_2O_3 (α) with 10 wt% Y_2O_3;	1747°C; 0 min dwell;	93 % TD	2.45 GHz Microwave
C1:	nano Al_2O_3 (γ) with 1 wt% CaO;	1100°C; 0 min dwell;	52 % TD	Conventional
C2:	nano Al_2O_3 (α) with 1 wt% CaO;	1530°C; 0 min dwell;	63 % TD	Conventional

Figure 2

7

2. Grain Growth during Sintering

Subsequent to each sintering run, the average particle size of the densified compact was determined from an x-ray diffraction measurement (Scherrer technique) [11]. Data for the pure nanocrystalline alumina, the nanocrystalline alumina with 10 wt% yttria, and the data from Ref. 7 (both XRD and BET results) are shown in Figure 3(B). Grain size is shown to increase rapidly with densification—10% densification of the green compact causes the grain size to increase from a few nanometers to > 50 nm. Grain sizes $\geq$ 1 μm are too large to be measured with the Scherrer method. The grain sizes obtained in the later stages of sintering the nanocrystalline alumina doped with 10 wt% yttria were estimated from SEM micrographs of the sintered workpieces. Micrographs of the 10 wt% yttria-doped samples are shown in Figure 6.

The data for the pure and yttria-doped alumina indicates that the increased densification with temperature is offset by increased grain growth. Consistent with the results of Ref. 7, our data shows that the initial increase in grain size is closely correlated with the γ to α-alumina phase transition. This transition occurs at about 100°C higher temperature in the pure alumina than in the yttria-doped alumina. Compared to the other dopants, the yttria containing samples had a greater amount of grain growth at lower temperatures than did the other additives except for the calcia-doped samples which showed 1 μm sized grains as low as 1200°C. This is probably due to the formation of CaO-Al_2O_3 eutectic that has a much lower melting temperature than does either CaO or Al_2O_3. This was confirmed by SEM's in which dense large CaO-rich hollow spheres were formed in relatively dense (84 %TD) Al_2O_3 of submicron-sized grains. Figures 7 and 8B show the results for the sintering of this material. Compacts sintered in a conventional tube furnace are included for comparison. Micrographs of these compacts are shown in Figure 8C. The magnesia doped samples showed the least amount of grain growth but also had the lowest sintered densities. This low grain growth was as expected as MgO is a grain-growth inhibitor.
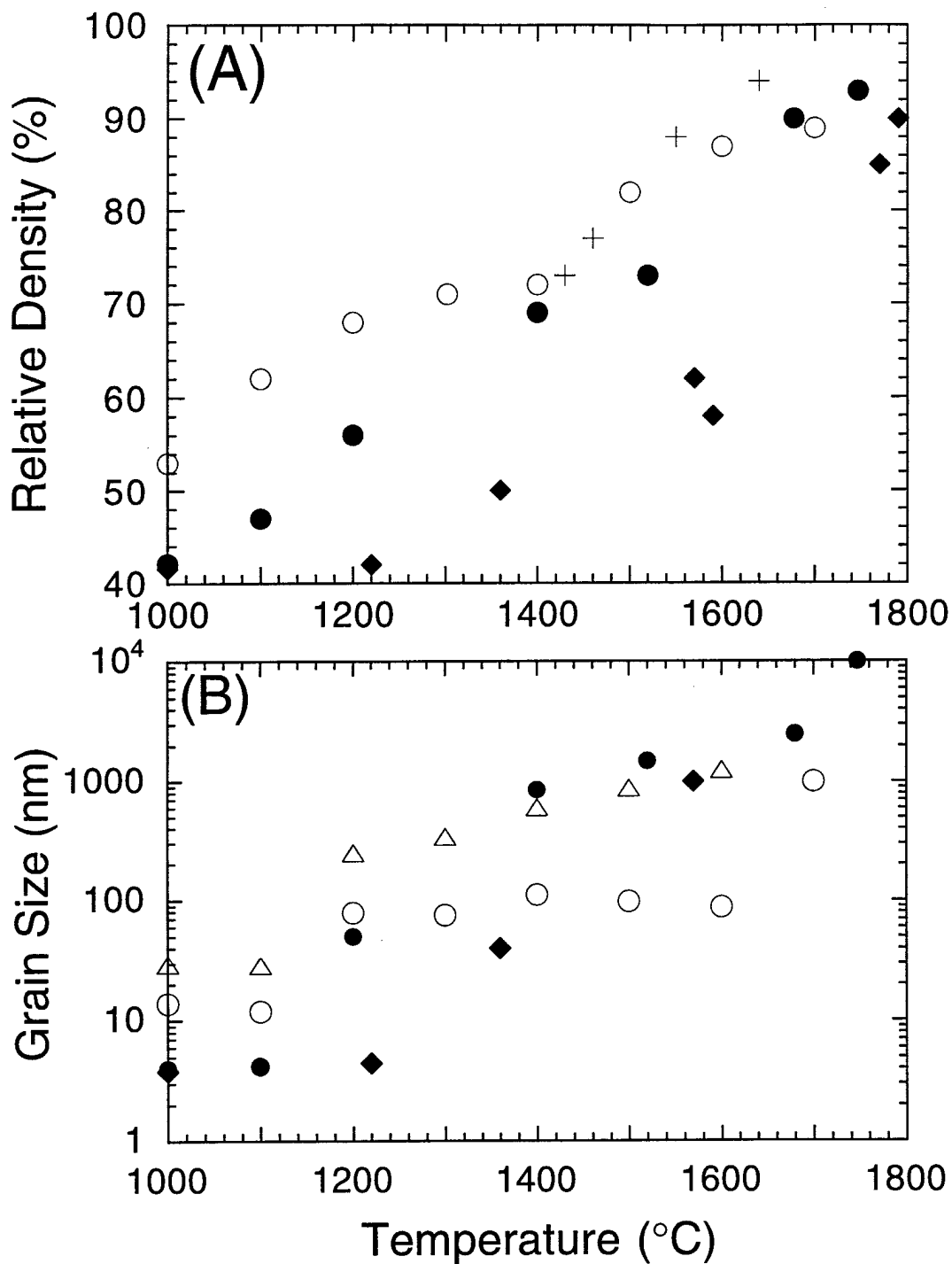
8

Figure 3. (A) Relative Density versus Temperature; (B) Grain Size versus Temperature.
{Legend: ◆: Pure nanocrystalline alumina; ●: nanocrystalline alumina with 10 wt%
yttria; ○: Data of Freim et al. [7] (grain size from XRD); △: Data of Freim et al. [7] (grain
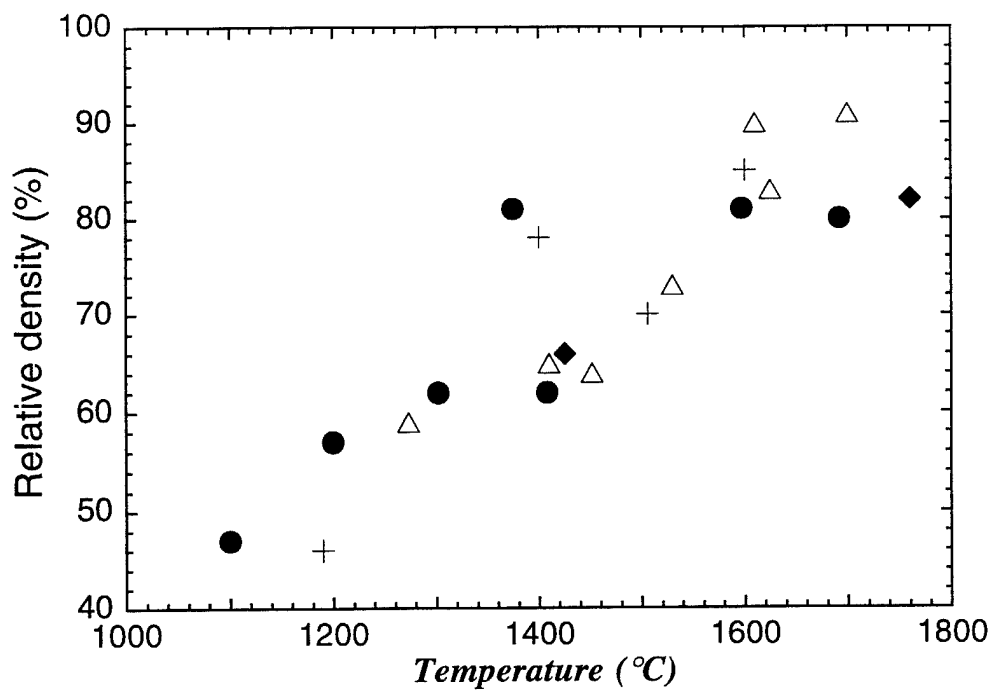size from BET); +:Data of Coble (60 minute hold) [10]}

9

Figure 4: Density versus temperature for nanocrystalline alumina with additives. Legend: +: 1 wt% yttria added in solution; : Δ 1 wt% yttria added as powder; ●: 1 wt% calcia added as powder; ◆: 1 wt% magnesia added as powder.

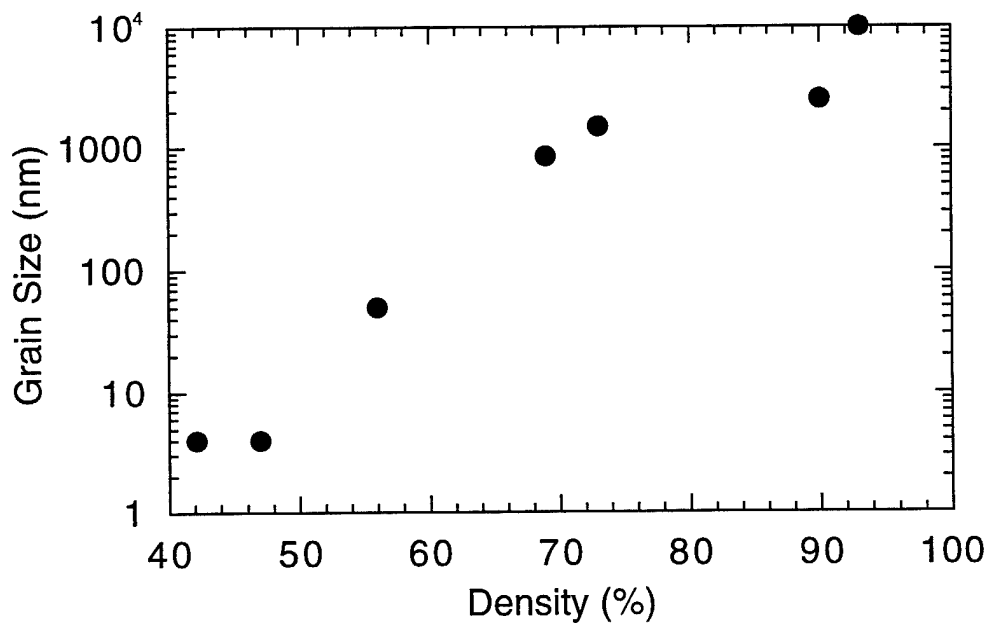Figure 5. Graph of grain size versus density for nAl_2O_3 + 10 wt% Y_2O_3.

3. Microscopy of Microwave Sintered Compacts

Figure 6 shows the development of microstructure in high purity, nanophase Al_2O_3 with 10 wt% Y_2O_3 added as a grain growth inhibitor, sintered to various temperatures in the 2.45 GHz microwave system, with essentially zero hold time. The microstructural development here is very similar to that seen in conventional sintering of aluminas. There is some sintering, primarily neck growth between particles, but little initial coarsening of the microstructure until the $\gamma - \alpha$ phase transformation temperature is reached (ca. 1250°C). At this point, the grain size increases to ca. 1 - 3 microns, and well-defined alpha-alumina grains are evident. Subsequent densification proceeds with associated grain growth, resulting in a nearly dense alumina body at sintering temperatures over 1600°C, with grain sizes approaching 10 - 20 microns at the densities corresponding to closed porosity (about 93% TD).

In Figure 8A, the results from similar experiments with additions of 1 wt% CaO are shown. Here the initial results are somewhat different, with more initial coarsening of the microstructure, and some indications of formation of glassy phases or low melting point phases. The grain facets visible in the 1375°C sintering experiment are not as well defined with rounded edges, again suggesting the presence of glassy phases. The temperatures here are below the melting points of any calcium aluminate phases, but above those of calcium silicates and calcium containing glasses. The final product here, at a peak sintering temperature of ca. 1600°C, has a grain size of about 2 - 5 microns, with density of only 81% TD; this is roughly the same density as that calculated from the yttria-doped alumina for the same temperature, thought the grain sizes for the calcia-doped material would appear to be somewhat larger.
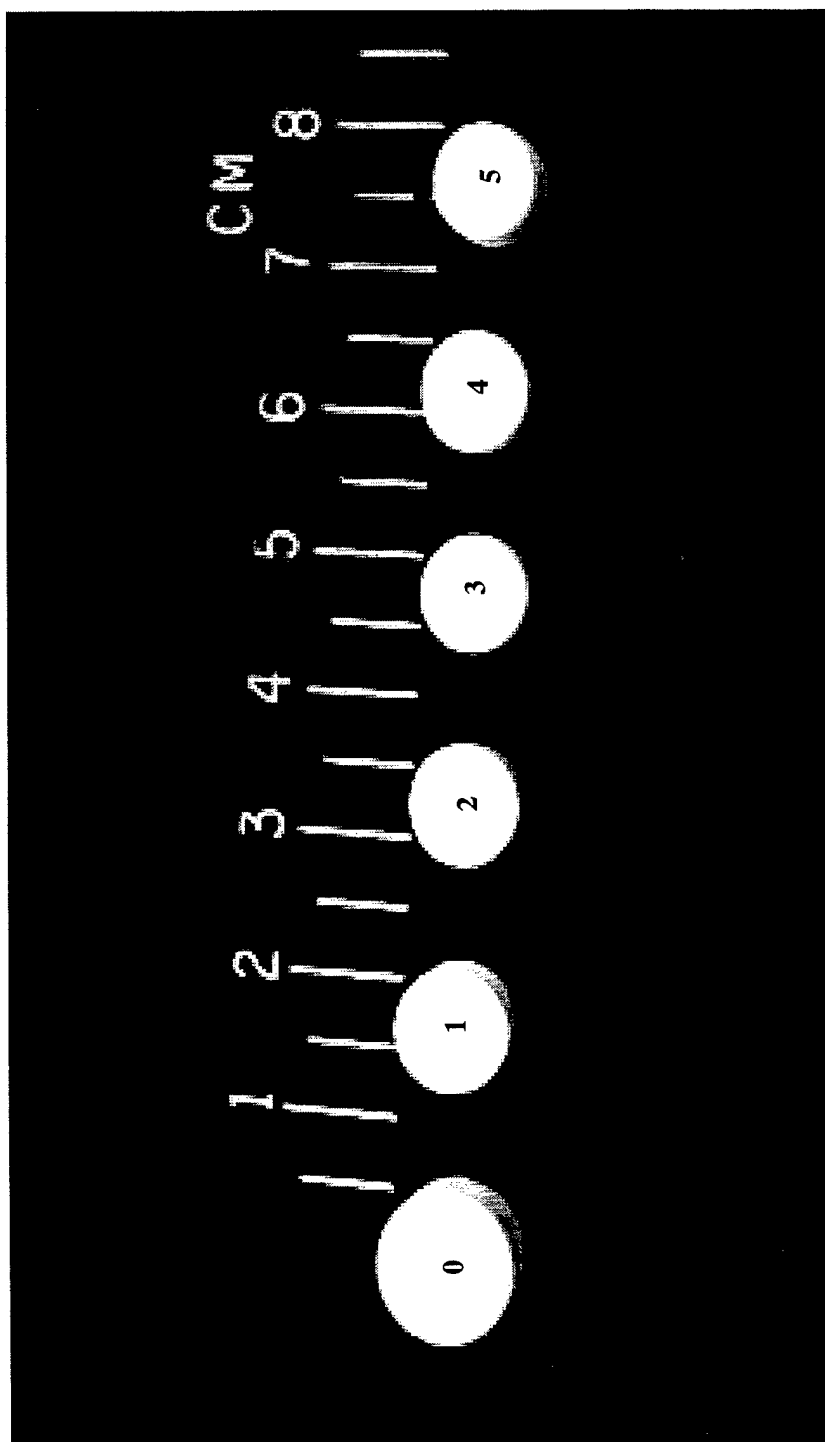
A more interesting result is shown in Figure 8B, again for calcia-doped nanophase alumina, but here showing the results of the heterogeneous distribution of the calcia within the alumina compact. The heterogeneous distribution is presumably the result of segregation of the calcia during drying and calcination of the powder, since the calcia was initially added in solution to the alumina precursor, and was initially very homogeneously distributed. The microwaves appear to couple preferentially to the calcia-rich regions, resulting in higher local temperature and local sintering. During this process, the calcia is drawn into the surrounding alumina material, resulting in the formation of roughly spherical pores surrounded by regions of dense, large grain alumina. This observation suggest that aluminas with controlled porosity could be produced by distribution of calcia particles of controlled size, followed by microwave sintering of the alumina. Note that

conventional sintering of calcia-doped alumina does not produce such effects as noted here, which are connected with the greater coupling of the microwaves to the CaO or the CaO-rich alumina regions, rather than just increased sintering of the alumina associated with the calcia doping. This difference is shown dramatically in Figure 8C, which illustrates comparable sintering results for calcia-doped alumina, using conventional sintering. Here actual agglomerates (Fig. 8C-3), presumably of CaO or CaO-rich alumina, are visible which, in this case sinter away from the surrounding alumina, and do not result in the formation of pores, as in the microwave case. Rather, the result is simply regions of higher density and larger grain size in the high temperature product. Thus there is fairly convincing evidence here of a microwave effect which might be put to use in other ways, i.e., enhanced coupling of microwave energy to additives with other beneficial effects of the same additives to produce unique microstructures unobtainable by conventional means.
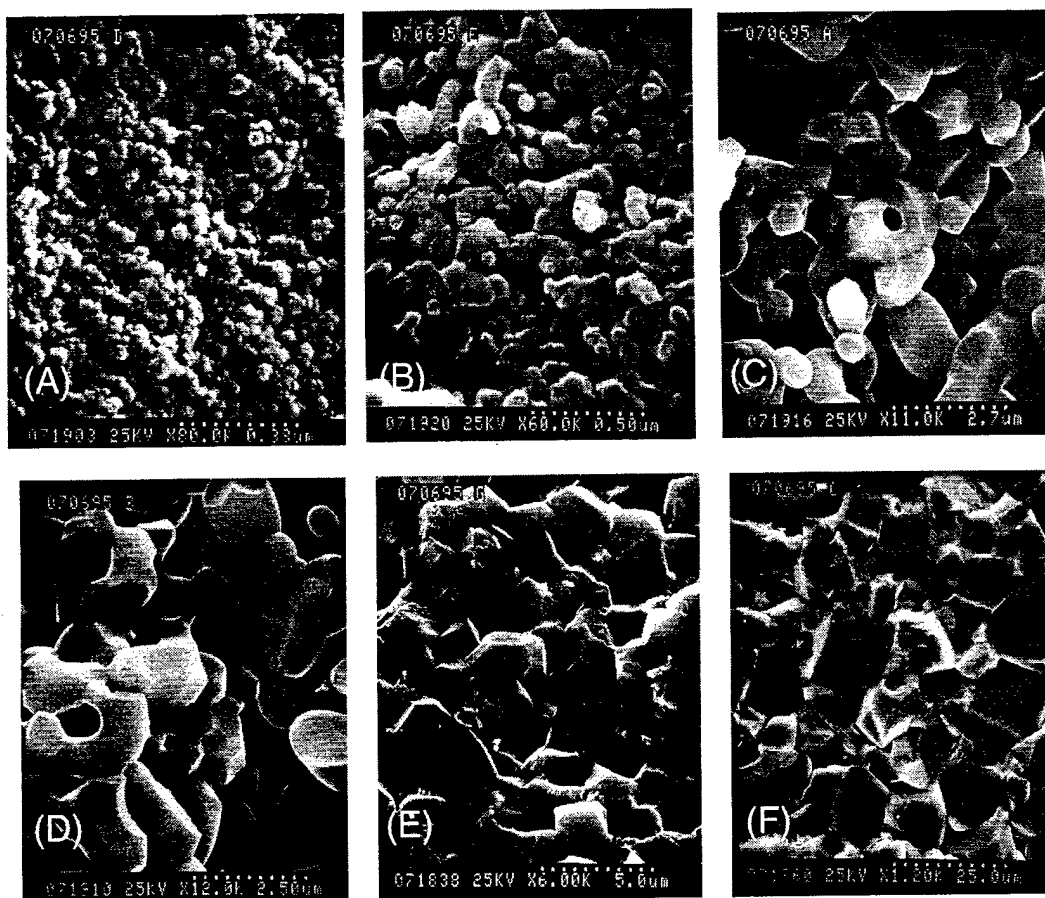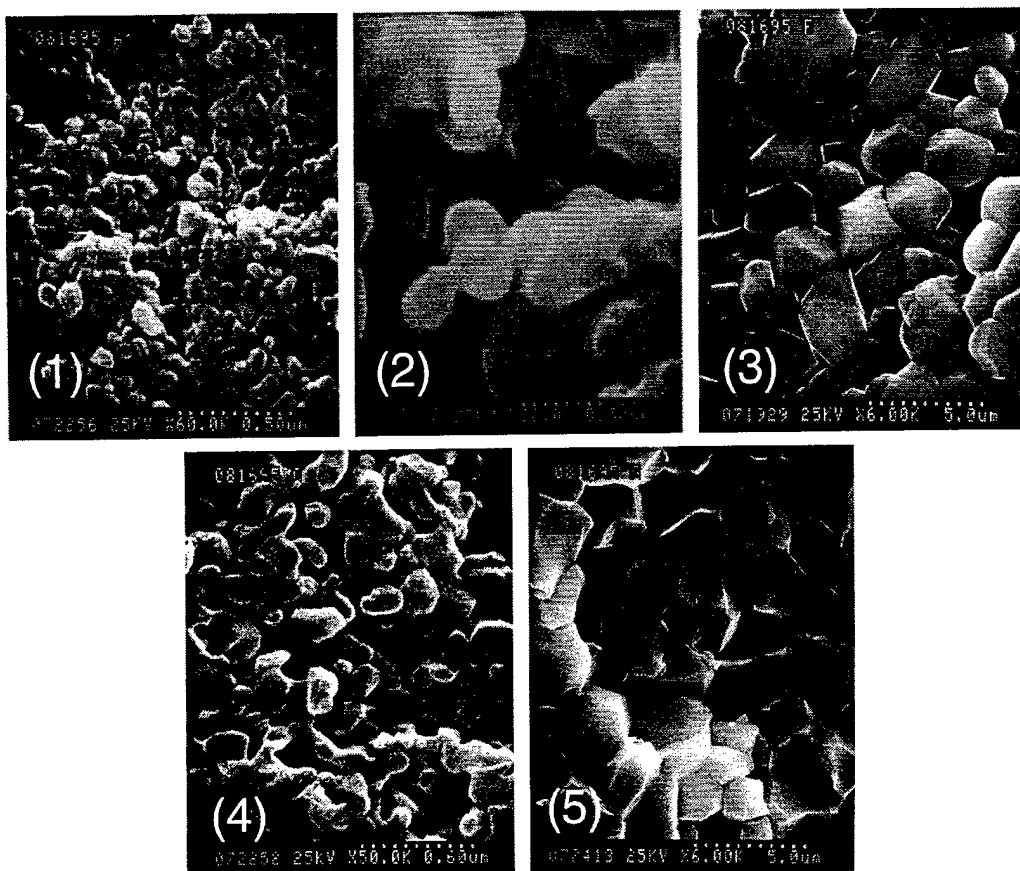
Micrograph	Temperature	Dwell (min)	%TD	Phase
A	1100°C	0	47	γ
B	1200°C	30	56	α
C	1400°C	0	69	α
D	1520°C	0	73	α
E	1678°C	0	90	α
F	1747°C	0	93	α

Figure 6. Scanning electron micrographs (SEM's) of nAl_2O_3 + 10 wt% Y_2O_3.
A: Shows the agglomerates of ~40 nm size consisting of ~ 4 nm sized grains (grain size determined from XRD); B: Beginning of neck formation, graininess of agglomerates diminishing showing formation of grains approximately the size of the agglomerates; C: Larger crystallites formed on the order of 1 μm; D: Well-formed grains and grain boundaries, some closed pores formed; E: Typical large dense crystallites with no internal pores showing absence of internal melting; F: Very large, ~ 10μm, grains formed of cubic structure, three orders of magnitude change in grain size from starting compact to a highly dense compact.

Sample 0:	Control: nano Al_2O_3 (γ)		Unprocessed, initial density	42 % TD
1:	nano Al_2O_3 (γ) with 1 wt% CaO;	1100°C; 0 min dwell;	Conventional Furnace	52% TD
2:	nano Al_2O_3 (α) with 1 wt% CaO;	1200°C; 0 min dwell;	2.45 GHz Microwave	57% TD
3:	nano Al_2O_3 (α) with 1 wt% CaO;	1375°C; 30 min dwell;	2.45 GHz Microwave	81% TD
4:	nano Al_2O_3 (α) with 1 wt% CaO;	1600°C; 0 min dwell;	2.45 GHz Microwave	81% TD
5:	nano Al_2O_3 (α) with 1 wt% CaO;	1692°C; 0 min dwell;	2.45 GHx Microwave	80% TD

Figure 7

Micrograph	Temperature	Dwell (min)	%TD	Phase
(1)	1200°C	0	57	α
(2)	1302°C	0	62	α
(3)	1375°C	30	81	α
(4)	1408°C	0	62	α
(5)	1597°C	0	81	α

Figure 8A. SEM's of nAl_2O_3 + 1 wt% CaO showing the fine grain structure of Al_2O_3 phases as a function of peak temperature and dwell time. (1): Grain growth has occured, original grain size was ~ 4nm, now ~0.1 μm; (2): Neck formation very evident and low density, still; (3): Long dwell time has resulted in significant densification but also significant grain growth; (4): Shorter dwell time but higher temperature still gives small grains (~0.2 μm) but low density; (5): Highest density achieved with highest temperature but large grains also.

Micrograph	Temperature	Dwell (min)	%TD	Phase
(1)	1302°C	0	62	α
(2)	1408°C	0	62	α
(3)	1597°C	0	81	α

Figure 8B. SEM's of nAl_2O_3 + 1 wt% CaO showing the effect of the preferential microwave heating of the CaO/Al_2O_3 mixture. Due to the eutectic temperature of $CaO-Al_2O_3$ (1390°C for an approximately 55-45% calcia-aluminate mixture) being much less than the melting temperature of either CaO (2580°C) or Al_2O_3 (2045°C) occlusions are formed at the boundary between the CaO and Al_2O_3. (1) Very good example of a hollow sphere with very dense CaO surrounding by nanophase α - Al_2O_3. Sphere is approximately 30 μm in diameter. Micrograph of the α - Al_2O_3 given in Figure 8A(2) showing grain sizes of approximately 0.2 μm. (2) Occulsion not as well defined due to possible extension of eutetic zone further into the nAl_2O_3, Micrograph of the α - Al_2O_3 given in Figure 8A(4) showing grain sizes of approximately 0.2 μm, similar to (1), above. (3): Significantly higher temperatures have resulted in the formation of acicular grains with a diameter of ~2 μm and a length of ~10 μm. Micrograph of the α - Al_2O_3 given in Figure 8A(5) showing grain sizes of approximately 2.0 μm. The lower processing temperature of (1) above suggests that well formed microspheres can be generated by selectively heating a mixture in which the eutectic temperature of the mixture is much less than the melting temperature of either component.
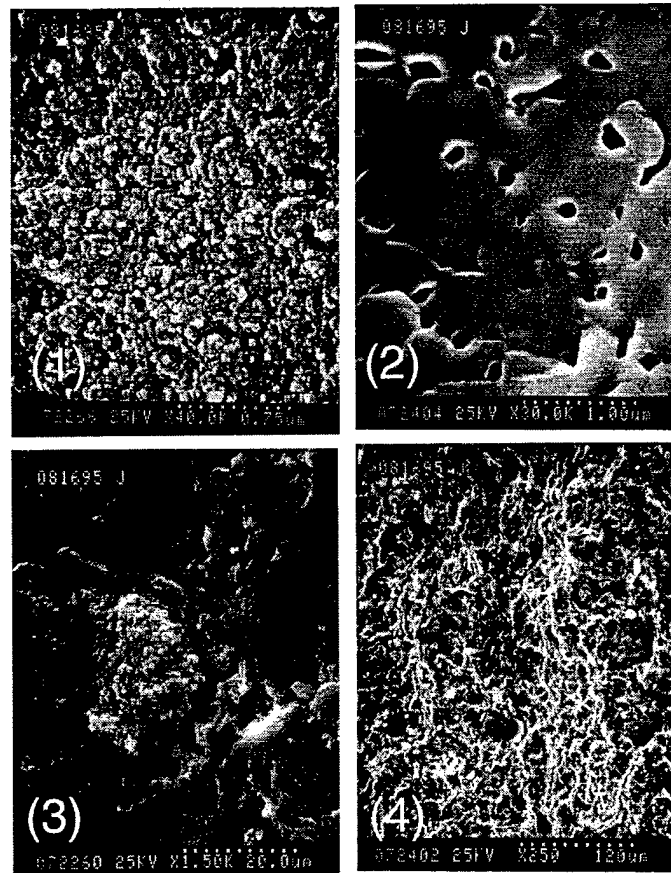
Micrographs	Temperature	Dwell (min)	%TD	Phase
(1)/(3)	1100°C	0	52	γ
(2)/(4)	1530°C	0	63	α

Figure 8C. SEM's of nAl_2O_3 + 1 wt% CaO showing the grain structure of Al_2O_3 phases as a function of peak temperature and dwell time for the conventionally sintered compacts. (1): Agglomerates of ultra-fine grains showing very little neck formation in keeping with the low temperature. Agglomerates are ~ 75 nm in size. Marginally densified compact. This contrasts with the higher temperature compact, (2), which shows significant grain growth and pore formation. The possibility of CaO agglomerate formation can be seen in (3) at 1100°C but there is little evidence of the products of these agglomerates at higher sintering temperatures, (4). This suggests that the conventional method of sintering does not have the preferential heating capability as does the microwave technique.

17

E. SUMMARY OF WORK

From the analysis of the data, the following points can be made:

- The use of additives leads to densification at lower temperatures, but this densification is achieved at the cost of increased grain growth.

- The rapid grain growth that occurs during the initial phases of sintering seems to correlate with the γ to α phase change in alumina. This agrees with the data of Freim et al. [7]

- The onset of the γ to α phase transition occurred approximately 100°C higher in the pure nanocrystalline alumina compared to those with additives. Freim et al. observed a similar difference between the phase transition temperature of their pressed and un-pressed powder. They attribute the lower temperature transition in the pressed powder to a greater number of nucleation sites. The presence of dopants may also increase the number of such nucleation sites.

- Preferential heating of a eutectic mixture may result in novel microstructures, e.g., CaO in nAl_2O_3.

One future goal of this study is to further explore the effect of calcination temperature upon agglomeration: lower calcination temperatures should yield less agglomeration and is the desired result. This should allow for higher green densities. Achieving the γ to α-alumina phase change without significant grain growth through an appropriate calcination method and/or microwave treatment will also be looked at. Finally, we intend to modify the cavity furnace to allow for an oxygen or vacuum environment to overcome the inhibiting effects upon densification due to the presence of nitrogen in the air atmosphere currently used [10].

III. The Role of Caskets/Insulators in Microwave Heating

A. INTRODUCTION

In the process of studying the microwave sintering of nanocrystalline alumina in a 2.45 GHz single-mode furnace, various insulating/hybrid schemes have been devised to promote the rapid and uniform heating and densification of the green compacts. These involve the use of caskets made of fiber board comprised of high-purity alumina, silica-coated alumina or yttria-stabilized zirconia, as well as the use of susceptor materials within the casket. The sintering process has proved to be sensitive to the casket material and configuration. In some cases, formation of hot spots in the casketing material led to thermal gradients in the compact resulting in cracking and non-uniform densification. In others, the casket material melted before the desired sintering temperature was reached. The best results were obtained using a casket system with a distributed susceptor/insulator material. In this section, the objectives are to discuss the choices to be made when putting together a microwave heating system and to stress the importance of thermal management.

B. INSULATING/SUSCEPTOR SYSTEMS

It must first be recognized that conventional methods of heating to sinter and densify ceramic powders approach thermal management from the outside in, i. e., the outside is hotter than the inside and the thermal energy must penetrate through the insulating layers to the workpiece. Microwave heating is the inverse situation with the inside hotter. This is especially true during the sintering of oxide ceramics in which the low thermal conductivity leads to an 'inverse' bathtub curve temperature profile. As a result, the objective is to keep the thermal energy from going to the usually far cooler walls of the microwave furnace. If this is not done properly, the thermal gradient generated by the very hot samples, sometimes > 1700 °C, between the interior and the cavity wall will significantly detract from the processing, resulting in cracked bodies and inefficient operation.

This was found to be especially true in the single-mode (TE_{103}) WR-284 microwave furnace used for the 2.45 GHz experiments and in the initial cavity used for
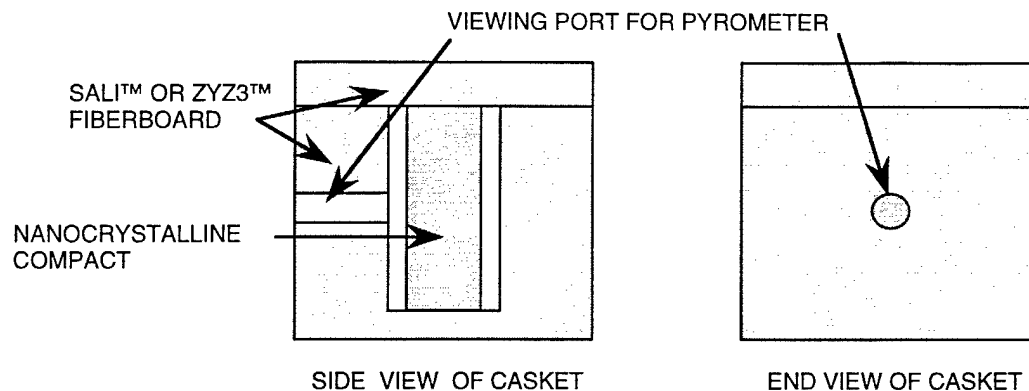
Figure 9. Original casket scheme for 2.45 GHz work.

35 GHz experiments. Because of the very limited space between the sample and the cavity surfaces (approximately 1.5 cm), only a minimal thickness of insulation was used [See Figure 9]. Thus thermal gradients on the order of 1000 °C/cm were obtained. Even for the best insulating materials used, significant thermal energy was lost to the cavity walls requiring increased power to the cavity to overcome these losses. Although this was not a particular problem for the 2.45 GHz system, as the available power from the Cober S6F source (6kW maximum) was sufficient, efficiency of the process was affected.

Another problem, besides the inefficient use of the supplied microwave power, was the need to use hybrid heating in the 2.45 GHz experiments. At the higher temperatures (>1500 °C), hot spots would form in the insulation resulting in a number of cases of thermal runaway. For some cases in which SiC powder was added as the susceptor material to the walls of the internal cavity in the Zircar AL-30™ insulation, thermal runaway would occur between these walls and the SiC powder, vitrifying the insulation. This can be seen in Figure 10. In the next example, Figure 11, thermal runaway also occurred in the AL-30™ insulation but this time the SiC powder partially densified causing further melting of the insulation. Another interesting case in shown in Figure 12 in which only partial thermal runaway occurred in the insulation. As is shown, the insulation vitrified/shrank in one area (top of right piece). This is of note because it shows the effect of how the microwave power will concentrate at the area of highest conductivity, the interface between the SiC and the insulation. For this example, the sample was highly densified.
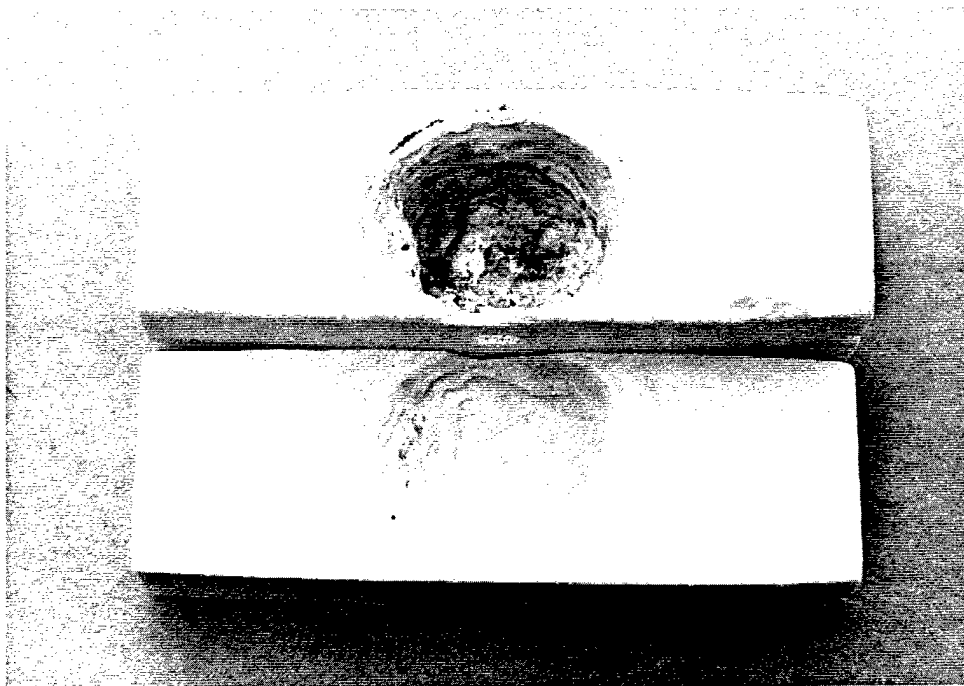
20

Figure 10. AL-30™ insulation. SiC was used as the susceptor but removed after the sintering run though some residue can be seen at the bottom of the upper piece. Notice the ovate shape of the vitrified area. Original hollowed out area (sample well) that contained the compact was much smaller.
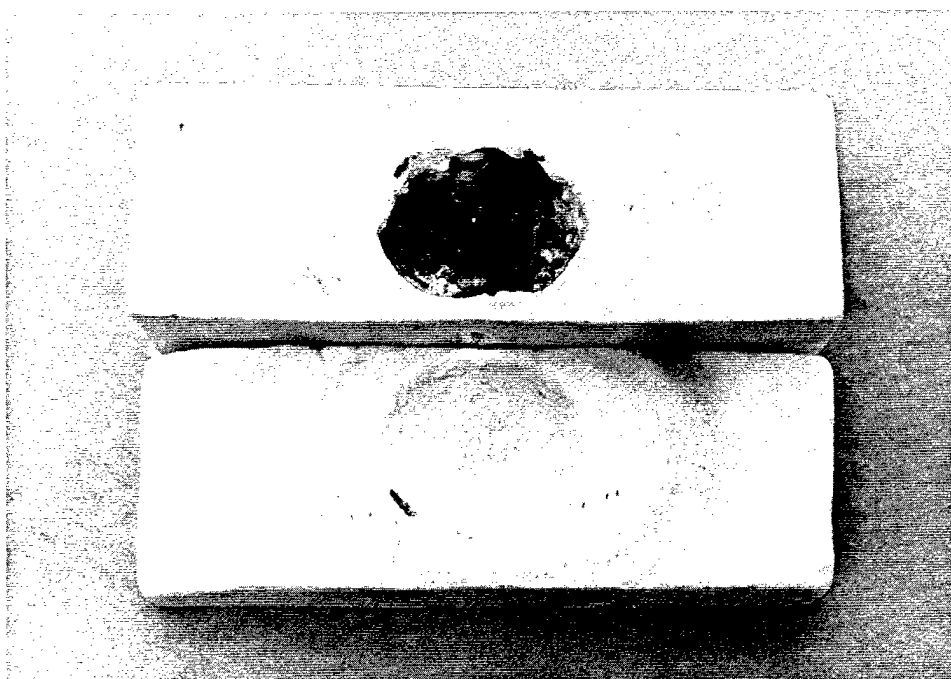

Figure 11. Al-30™ insulation with SiC powder as the susceptor. Similar ovate volume produced with some densification of the SiC powder. Increased melting of the insulation in the upper piece.
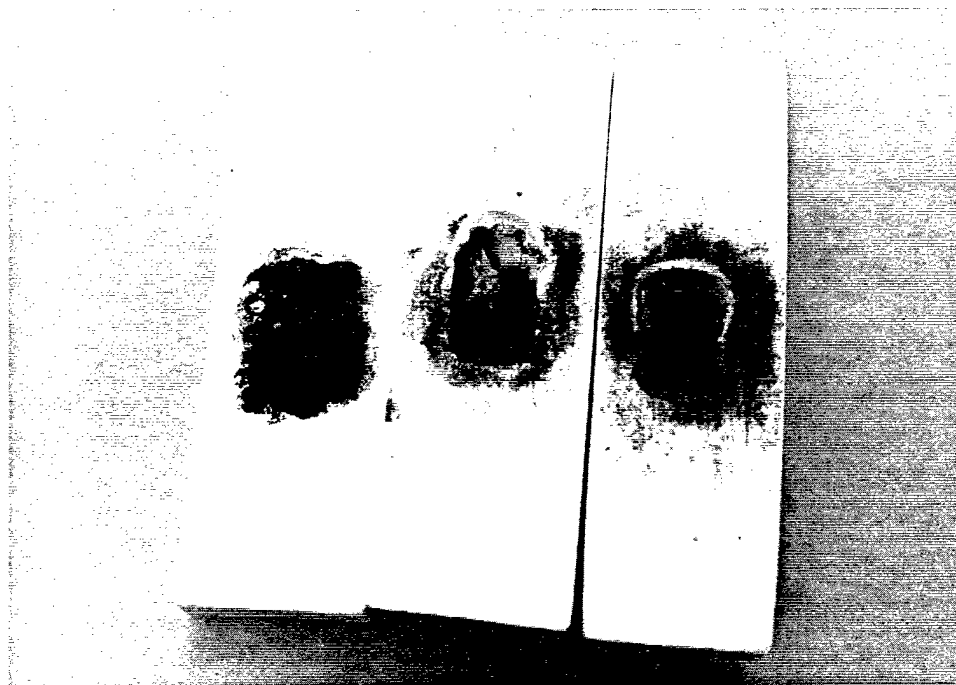
Figure 12. AL-30™ insulation with SiC powder as the susceptor. Notice that the SiC coating of sample well is mostly intact but shrinkage/densification of the AL-30™ insulation and partial densification of the SiC powder. Sample was highly densified.

Zircar SALI™ insulation was then used in conjunction with the SiC powder and Zircar ZYZ3™ yttria stabilized zirconia (YSZ) pieces placed around the inside of a hollowed-out cavity in the insulation, Figure 13. But due to thermal runaway, the YSZ melted into the SALI™. This is shown at the top of the figure. Although there was thermal runaway in the insulation, the compact was highly densified.

In order to alleviate some of the problems associated with the use of an insulation that also acted as absorber, a casket based on Zircar SALI™ insulation with an absorbing/insulating powder made of boron nitride (BN) and glassy carbon (GC) was used [12]. The SALI™ insulation is very transparent to microwaves and has a high service temperature (>1700°C) which makes it ideal for most of the applications being studied. The BN/GC mixture is a unique material because the BN is very transparent to microwaves, has a service temperature greater than 2200 °C and is a very good thermal insulator. The glassy carbon is a good conductor and normally would reflect the energy away from the compact. But when the BN and GC are mixed in the proper ratio, the mixture acts as a very good distributed insulator/susceptor. At low temperatures, the
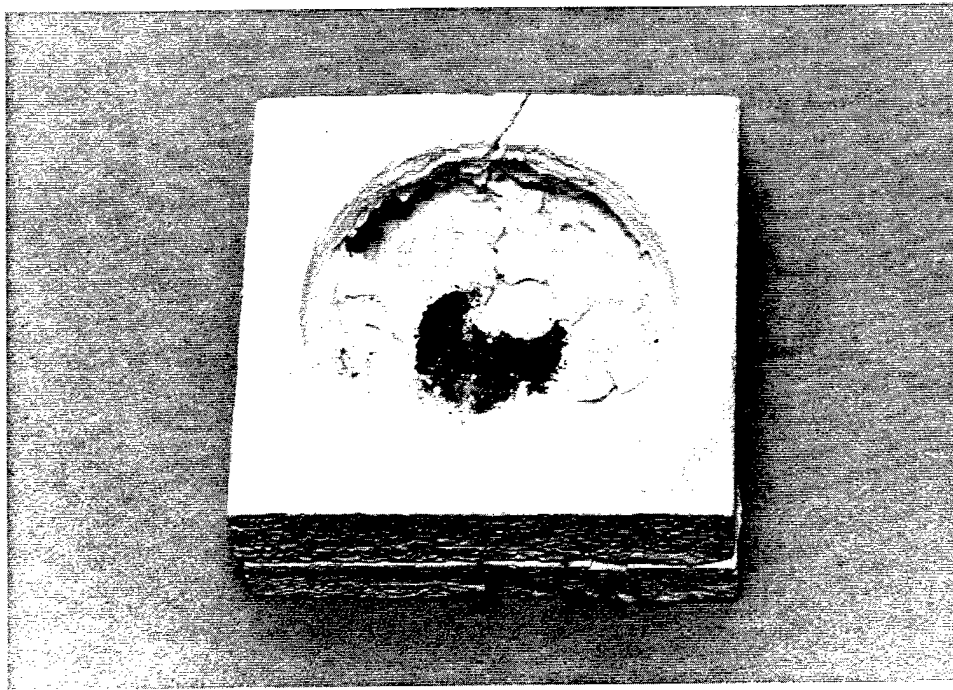
Figure 13. SiC powder with Zircar ZYZ3™ yttria stabilized zirconia (YSZ) in a Zircar SALI™ casket. SiC powder placed in center on which the sample is placed. Around this was placed small pieces of YSZ insulation. The YSZ melted into the SALI insulation during thermal runaway. Insulation cracked and melted. Sample was highly densified.

mixture acts as the hybrid heater transferring heat to the compact. At higher temperatures, the compact is very absorbing compared to the mixture and is thus self heating. The BN then acts as a very good insulator. The first attempts at using this material, though, had some of the same problems with thermal runaway. In Figure 14 is shown a case in which the glassy carbon got sufficiently hot to melt the SALI™ insulation. The piece on the right contained the BN/GC mixture with the compact embedded in the middle. The top of this piece shows evidence of thermal runaway in which the GC caused the insulation to melt. It should be noted that this side of the insulation was in the direction of the source and thus saw the highest fields.
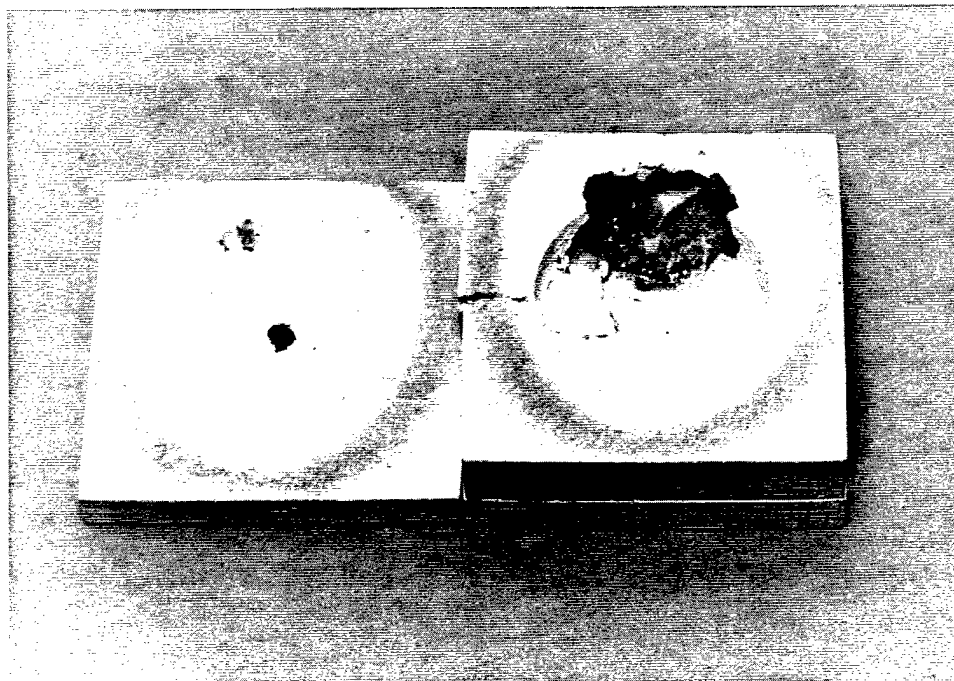
Figure 14 Use of BN/GC as the susceptor/first insulation level. Thermal runaway on source side of casket. Black material is principally glassy carbon plus some BN powder residue with vitrification/melting of the SALI™ insulating material.

In order to isolate the BN/GC mixture from the insulation, a fully dense alumina crucible was used to contain the mixture and was placed in a hollowed-out cavity within the insulation, Figure 15. Several successful runs were made with this scheme but on the final run, thermal runaway was again encountered. It is apparent that hot spots formed at the boundary between the alumina crucible and the insulation. In Figure 15, the initial hot spot formed on the source side of the insulation (top of each insulation piece). This caused melting not only of the insulation but also of the crucible which indicates that temperatures above 2200°C were reached. It should also be noted that a very clear line of melting is evident in the crucible (right piece). This line is along the axis of the microwave power flow and clearly indicates that the high field strengths are concentrated in the middle of the cavity along this axis.
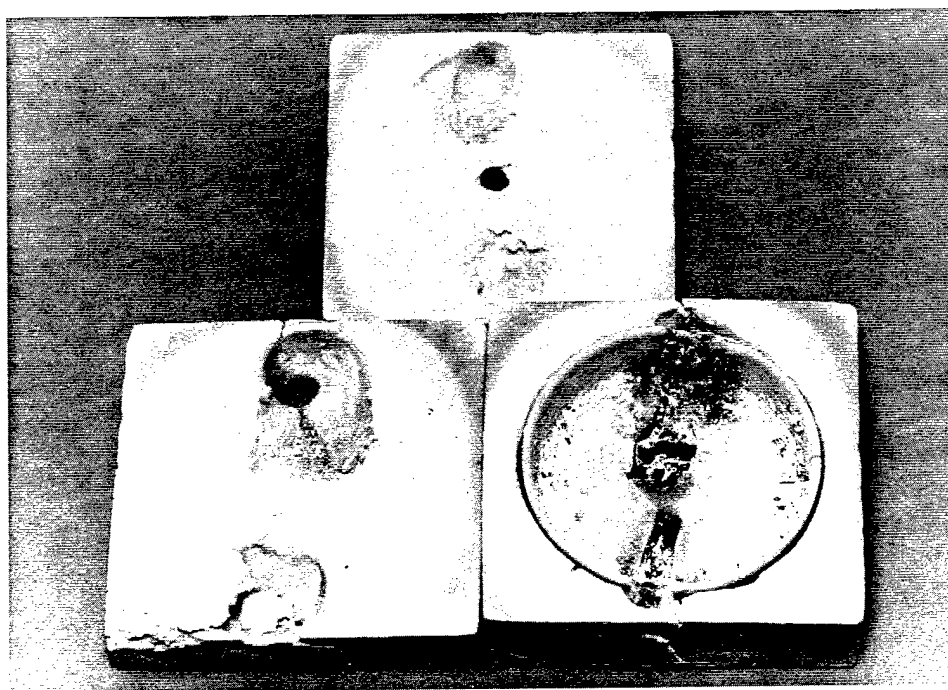
Figure 15. Triple layer of SALI™ insulation with center piece hollowed out to receive 2" diam. alumina crucible. Crucible filled with BN/GC mixture . Piece to left is bottom layer, top piece is top (inverted to indicate melting). Melting of insulation and alumina crucible. Top of crucible was the microwave source direction, bottom toward the variable short. Notice that the melting occurred along the center line where the field was a maximum. Melting of the SALI™, alumina + BN/GC together. Observed temperature of the nanocrystalline alumina sample was approximately 1800 °C, but it is obvious that much higher temperatures were obtained.

An example of successful densification and sintering is shown in Figure 16 (A and B). As can be seen in this figure, the compact is completely surrounded by the BN/GC mixture except for the top. When the top of the casket (insulation piece to the left of the figure) is placed over the sample, the temperature is monitored through the hole. Although there is some radiative heat loss through this aperture, it is not sufficient to distort the temperature readings.

Although this configuration was successful for many of the sintering experiments conducted, it was not entirely successful when trying to obtain temperatures above 1700 °C. Any perturbation in the heating could possibly cause thermal runaway in that portion exposed to the highest fields (see Figure 15). As a result, two other casketing schemes were tried. The first consisted of a boron nitride crucible containing the BN/GC mixture. The compact was placed into the mixture with an aperture for temperature
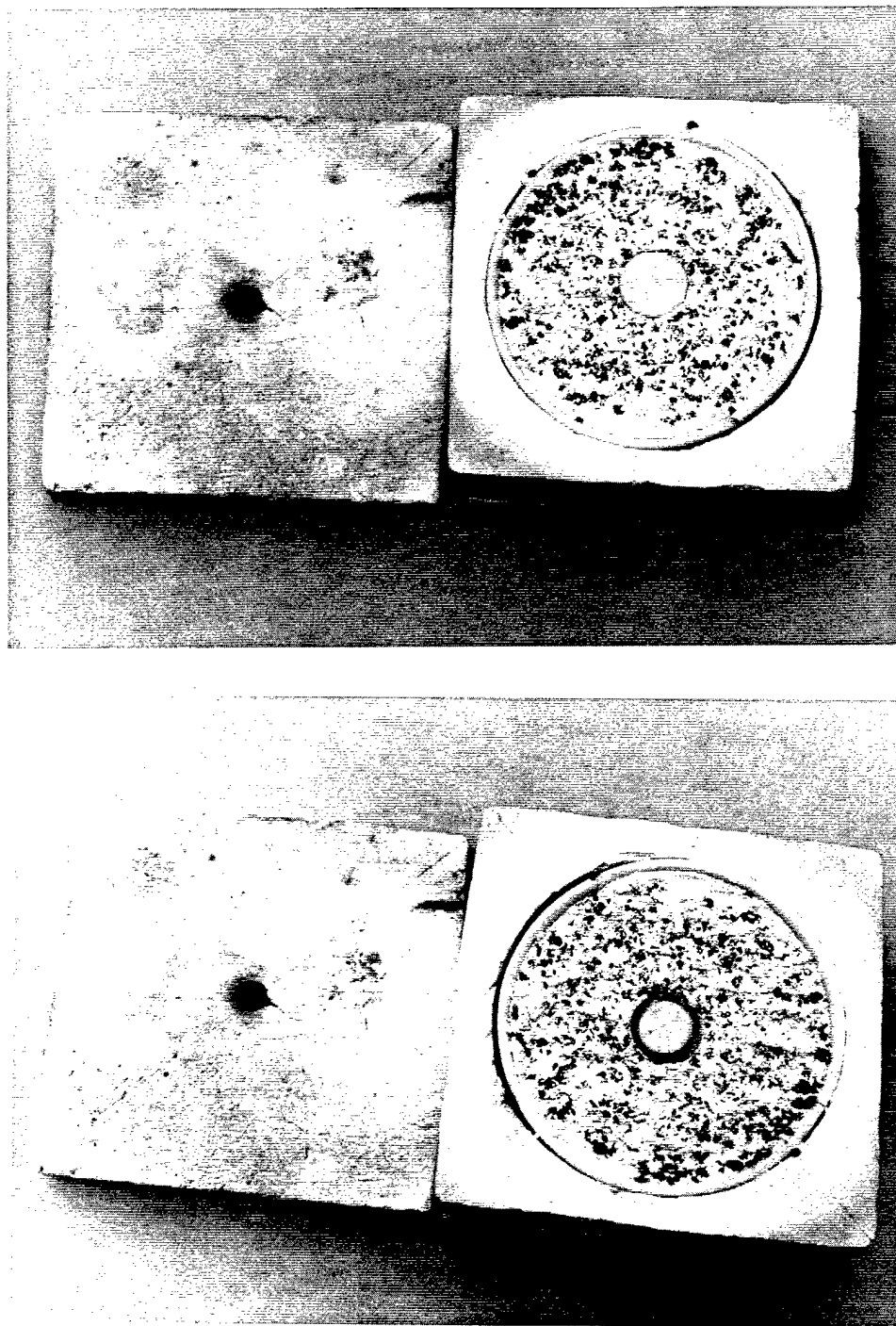
Figure 16. A (top): Arrangement of compact in BN/GC mixture inside of alumina crucible contained in a SALI™ casket. Note that the compact is in complete contact with the mixture. B (bottom): Successful densification and sintering. Notice the amount of shrinkage obtained in the compact.

monitoring. In this case, the mixture covered all sides except for the aperture. This assemblage was then placed in Zircar FBD™ YSZ insulation. This insulation, which is somewhat denser than the Zircar ZYZ3™ insulation has even better high temperature characteristics (maximum use temperature of 2200 °C, melting temperature of 2590 °C vice 1700 °C maximum use temperature [intermittent] and melting temperature of 2200 °C for ZYZ3™). But due to the increased lossiness of this insulation, it absorbed the microwave power more than did the compact. Although the power was increased, the compact did not significantly heat. Fortunately, the insulation did not degrade and go into thermal runaway.

The second scheme was to use the assemblage with a dense piece of alumina for a base to insulate it from the cavity bottom wall (See Figure 17). This combination proved the most successful and did not exhibit thermal runaway.
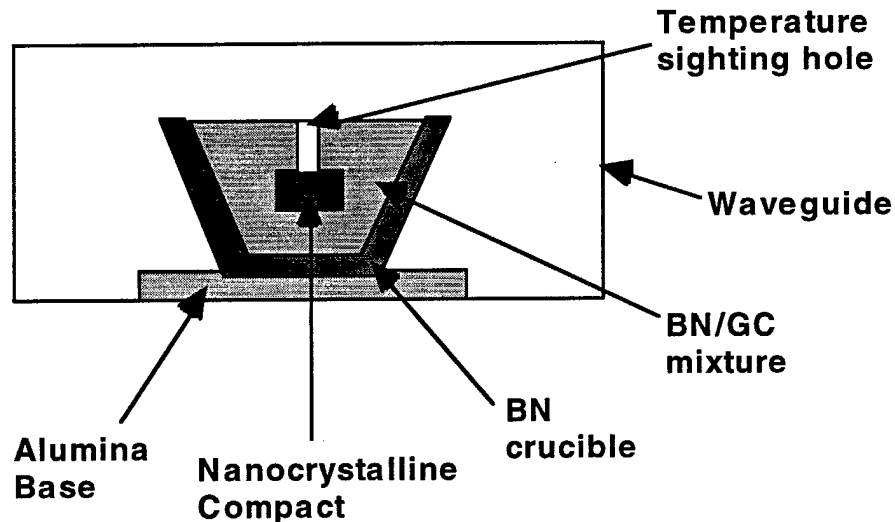

Figure 17. Transverse view of the arrangement of the BN crucible containing the compact and the BN/GC mixture. Note the temperature sighting hole which is just an aperture made in the powder mixture.

C.   SUMMARY

Various insulating and hybrid heating schemes have been used in the sintering and densification of pure and doped nanocrystalline alumina. From simple systems in which the insulation (Zircar ZYZ3™) was both hybrid heater and insulation, to more elaborate ones in which a mixture of boron nitride and glassy carbon contained in a BN crucible proved the most successful. In all but the last case, thermal runaway proved to

be a constant problem when trying to heat to temperatures above 1700 °C. In this latter case, though, the system has some room for improvement as the BN crucible still radiates significant thermal energy to the surrounding cold-walled microwave cavity environment. This has not been a problem at 2.45 GHz because there is adequate power and could be further reduced by using a larger multi-mode furnace.

IV. Summary of Work at 2.45 GHz

The work accomplished to date at 2.45 GHz has centered on the sintering of nanocrystalline metal-oxide (alumina and titania) ceramics. In the original planning for these studies it was hoped that these materials could be sintered without the use of sintering aids or hybrid heating. Although sintering aids, per se, have not been used other than looking at the effect of dopants on sintering behavior, hybrid heating has been universally used at this frequency. Based upon the high defect concentration on the surface of nanon-sized[†] particles, it had been expected that direct coupling would have occurred. Since this did not happen, i.e., the effect of increased conductivity at this frequency was not enough, much higher frequencies would be required in order to overcome the low room temperature heating capability of these materials. Experiments at a higher frequency, 35 GHz, have been accomplished and show that at this frequency, HF microwave energy can directly couple to nanon-, submicron- and micron-sized grains without hybrid heating [15-16].

V. Acknowledgment

References

1. A. W. Fliflet, R. W. Bruce, D. Lewis, III, R. Rayne, B. Bender, L. K. Kurihara, G.-M. Chow, P. E. Schoen and A. K. Kinkead, "Design and Initial Operation of a 6 kW 2.45 GHz Single-Mode Microwave Cavity Furnace," NRL Memorandum Report NRL/MR/6793--95-7745, 1995.
2. R. W. Bruce, A. W. Fliflet, L. K. Kurihara, D. Lewis, III, R. Rayne, G.-M. Chow, P. E. Schoen, B. A. Bender and A. K. Kinkead in *Microwaves: Theory and Applications in Materials Processing III*, edited by D. E. Clark, D. C. Folz, S. J. Oda, and R. Silberglitt (*Amer. Cer. Soc.. Trans.* **59**, Westerville, OH, 1995) pp. 407-414.
3. W. H. Sutton, *MRS Bulletin* **23** (11), (1993).

[†] "nanon" : nanometer sized, similar to "micron" being used for micrometer-sized.

4. M. Aliquat, L. Mazo and G. Desgardin in *Microwave Processing of Materials II,* edited by W. B. Snyder, Jr., W. H. Sutton, M. F. Iskander and D. L. Johnson (*Mater. Res. Soc. Proc.* **189**, Pittsburgh, PA, 1991) pp. 229-235.

5. J. A. Eastman, K. E. Sickafus, J. D. Katz, S. G. Boeke, R. D. Blake, C. R. Evans, R. B. Schwarz and Y. X. Liao in *Microwave Processing of Materials II*, edited by W. B. Snyder, Jr., W. H. Sutton, M. F. Iskander and D. L. Johnson (*Mater. Res. Soc. Proc.* **189**, Pittsburgh, PA, 1991) pp. 273-278.

6. D. Vollath, R. Varma and K. E. Sickafus in *Microwave Processing of Materials III*, edited by R. L. Beatty, W. H. Sutton and M. F. Iskander (*Mater. Res. Soc. Proc.* **269**, Pittsburgh, PA, 1992) pp. 379-384.

7. J. Freim, J. McKittrick, J. Katz and K. Sickafus in *Microwave Processing of Materials IV,* edited by M. F. Iskander, R. J. Lauf and W. H. Sutton (*Mater. Res. Soc. Proc.* **347**, Pittsburgh, PA, 1994) pp. 525-530.

8. L. K. Kurihara, G.-M. Chow and P. E. Schoen, "Low Temperature Processing of Nanoscale Ceramic Nitride Particles Using Molecular Precursors," Patent Disclosure, US Navy Case 82,737 (1995), application pending.

9. R. W. Bruce, A. W. Fliflet and A. K. Kinkead, " Insulating/Hybrid Heating Systems for Microwave Sintering Experiments," presented at the 1996 MRS Spring Meeting, San Francisco, CA, 1996 (unpublished).

10. R. L. Coble, *J. Amer. Cer. Soc.* **45**, 123 (1962)

11. B.D. Cullity, *Elements of X-RAY DIFFRACTION*, 2nd ed., Addison-Wesley Publishing Co., Reading, MA, 1978, pp. 98-102, 284-285.

12. M.S. Morrow, ORNL,/Lockheed-Martin, private communication.

13. A.W. Fliflet, R.P. Fischer, A.K. Kinkead and R.W. Bruce in *Microwave Processing of Materials V,* edited by M. F. Iskander, J.O. Kiggans and J.-C. Bolomey (*Mater. Res. Soc. Proc.* **430**, Pittsburgh, PA, 1996) pp. 527-532.

14. R.W. Bruce, A.W. Fliflet, R.P. Fischer, D. Lewis, III, B.A. Bender, R.J. Rayne, L.K. Kurihara, G.-M. Chow and P.E. Schoen, "Millimeter-Wave Processing of Alumina Compacts," to be published in *Ceramic Transactions*, Vol. 80, W.H. Sutton, D.E. Clarke, and D.A. Lewis, ed., 1997

15. A.W. Fliflet, R.P. Fischer, R.W. Bruce, and A.K. Kinkead, "Gyrotron-Based Millimeter-Wave Furnaces for Ceramic Sintering," presented at the First World Congress on Microwave Processing, Lake Buena Vista, FL, January 3-5, 1997.